LETTER

https://doi.org/10.1038/s41586-018-0726-6

A structural transition in physical networks

Nima Dehmamy[1], Soodabeh Milanlouei[1] & Albert-László Barabási[1,2,3]*

In many physical networks, including neurons in the brain[1,2], three-dimensional integrated circuits[3] and underground hyphal networks[4], the nodes and links are physical objects that cannot intersect or overlap with each other. To take this into account, non-crossing conditions can be imposed to constrain the geometry of networks, which consequently affects how they form, evolve and function. However, these constraints are not included in the theoretical frameworks that are currently used to characterize real networks[5–7]. Most tools for laying out networks are variants of the force-directed layout algorithm[8,9]—which assumes dimensionless nodes and links—and are therefore unable to reveal the geometry of densely packed physical networks. Here we develop a modelling framework that accounts for the physical sizes of nodes and links, allowing us to explore how non-crossing conditions affect the geometry of a network. For small link thicknesses, we observe a weakly interacting regime in which link crossings are avoided via local link rearrangements, without altering the overall geometry of the layout compared to the force-directed layout. Once the link thickness exceeds a threshold, a strongly interacting regime emerges in which multiple geometric quantities, such as the total link length and the link curvature, scale with the link thickness. We show that the crossover between the two regimes is driven by the non-crossing condition, which allows us to derive the transition point analytically and show that networks with large numbers of nodes will ultimately exist in the strongly interacting regime. We also find that networks in the weakly interacting regime display a solid-like response to stress, whereas in the strongly interacting regime they behave in a gel-like fashion. Networks in the weakly interacting regime are amenable to 3D printing and so can be used to visualize network geometry, and the strongly interacting regime provides insights into the scaling of the sizes of densely packed mammalian brains.

To lay out physical networks, the links and nodes must be arranged in such a way to avoid crossing each other, while minimizing the total length of the links, because long links can be costly in systems such as brains. In other words, we must find the shortest path for each link, which may not be a straight path if the straight path is obstructed by other nodes and links—a problem that is equivalent to stretching a rubber band between flexible obstacles (Fig. 1; see Supplementary Information section 3.A for a proof of this equivalence[10]).

To find the shortest path, we propose a model in which the forces that govern the motion of the nodes and links are determined by the gradient of the total potential energy. We define the total potential energy as:

$$\begin{aligned} V &= V_{\mathrm{el}} + V_{\mathrm{NL}} + V_{\mathrm{NN}} + V_{\mathrm{LL}} \\ &= \frac{k}{2}\sum_l \int \left|\frac{\mathrm{d}\boldsymbol{x}_l}{\mathrm{d}s_l}\right|^2 \mathrm{d}s_l + k\sum_{i=1}^{N}\sum_{l\in\langle i\rangle} \boldsymbol{X}_i\cdot\frac{\mathrm{d}\boldsymbol{x}_l}{\mathrm{d}s_l}\Bigg|_{s_l=s_l^{(\mathrm{end})}} \\ &\quad + A_{\mathrm{N}}\sum_{i\neq j}\exp\left(-\frac{|\boldsymbol{X}_i-\boldsymbol{X}_j|^2}{4r_{\mathrm{N}}^2}\right) + A_{\mathrm{L}}\sum_{l\neq m}\int\int \exp\left(-\frac{|\boldsymbol{x}_l-\boldsymbol{x}_m|^2}{4r_{\mathrm{L}}^2}\right)\mathrm{d}s_l\mathrm{d}s_m \end{aligned} \tag{1}$$

where V_{el} is the total elastic potential of all links ($l=1,\ldots,L$). Each link is modelled as an elastic cylinder with radius r_{L}, which experiences internal elastic forces and short-range external repulsive forces from other links and nodes; nodes are modelled as spheres. V_{NL} captures the node–link interactions at the endpoints of the links; the non-crossing condition is ensured by a short-range repulsive force in the node–node interaction V_{NN} and in the link–link interaction V_{LL}, which are both modelled as short-range Gaussian potentials with strengths set by A_{N} and A_{L}, respectively. In addition, s_l parameterizes the length of link l, with $s_l^{(\mathrm{end})}$ denoting its endpoint; $\boldsymbol{x}_l(s_l, t)$ is the position of a point along the centre of link l at time t; $\boldsymbol{X}_i(t)$ is the position of node i ($i=1,\ldots,N$); r_{N} is the range of the node–node repulsive force; k is the elastic constant of the links; and $l\in\langle i\rangle$ indicates that the sum is over all links connected to node i. The potential energy in equation (1) is inspired by models used in self-avoiding polymer chains[11] and manifold dynamics[12]; however, given the constraints induced by the network structure, equation (1) has different terms and describes behaviour that is unique to networks.

With $V_{\mathrm{LL}}=0$ and replacing V_{el} with the elastic energy of a spring, equation (1) reduces to the potential energy of a force-directed layout (FDL) with short-range node repulsion. The lowest-energy solution of equation (1) can involve sharp bending of some links, which we avoid by using a Gay–Berne potential[13], as in polymer physics (Supplementary Information section 4). Finally, we embed the network in a high-viscosity medium, allowing it to relax to a low-energy state without oscillations. Therefore, the node and link positions (X_i and x_l) follow the first-order gradient-descent equations of motion:

$$\lambda_{\mathrm{N}}\frac{\mathrm{d}X_i}{\mathrm{d}t} = -\frac{\partial V}{\partial X_i}; \quad \lambda_{\mathrm{L}}\frac{\mathrm{d}x_l}{\mathrm{d}t} = -\frac{\partial V}{\partial x_l} + \frac{\mathrm{d}}{\mathrm{d}s_l}\frac{\partial V}{\partial(\mathrm{d}x_l/\mathrm{d}s_l)} \tag{2}$$

where λ_{N} and λ_{L} are the friction constants of the nodes and links (Supplementary Information section 3.F). We use an FDL to set the initial positions of the nodes and explore two versions of the model with different constraints: (i) in the elastic-link model (ELI), which corresponds to the limit $\lambda_{\mathrm{N}}\to\infty$, the positions of the nodes are fixed and only the links can reorganize; (ii) in the fully elastic model (FUEL), we assume that $\lambda_{\mathrm{N}}\approx\lambda_{\mathrm{L}}$ and hence the nodes and links are all free to move.

The network defined by equations (1) and (2) has an uneven potential-energy landscape[14] with a very large number of local minima; identifying the globally optimal configuration is NP hard (Supplementary Information section 3.G). We therefore use simulated annealing[15] to approach an energetically favourable local minimum (Supplementary Information section 3.G). The computational complexity of the model is discussed in Supplementary Information section 8.C. In Fig. 1c we show how FUEL finds the optimal three-dimensional configuration of a lattice, helped by the thermal fluctuations from simulated annealing that were added to the links, which allow the layout to tunnel through the finite potential walls and escape local minima.

Because FDLs do not take into account the physical dimensions of the nodes and links, they typically have multiple link and node crossings (Supplementary Information section 2). The number of crossings increases linearly with r_{L} (Fig. 2a), as predicted analytically by a geometric model (Supplementary Information section 2). To avoid these crossings, we applied ELI and FUEL to several networks with different topologies (random networks and Barabási–Albert[16] scale-free

[1]Network Science Institute, Center for Complex Network Research, Department of Physics, Northeastern University, Boston, MA, USA. [2]Division of Network Medicine, Brigham and Women's Hospital, Harvard Medical School, Boston, MA, USA. [3]Department of Network and Data Sciences, Central European University, Budapest, Hungary. *e-mail: alb@neu.edu

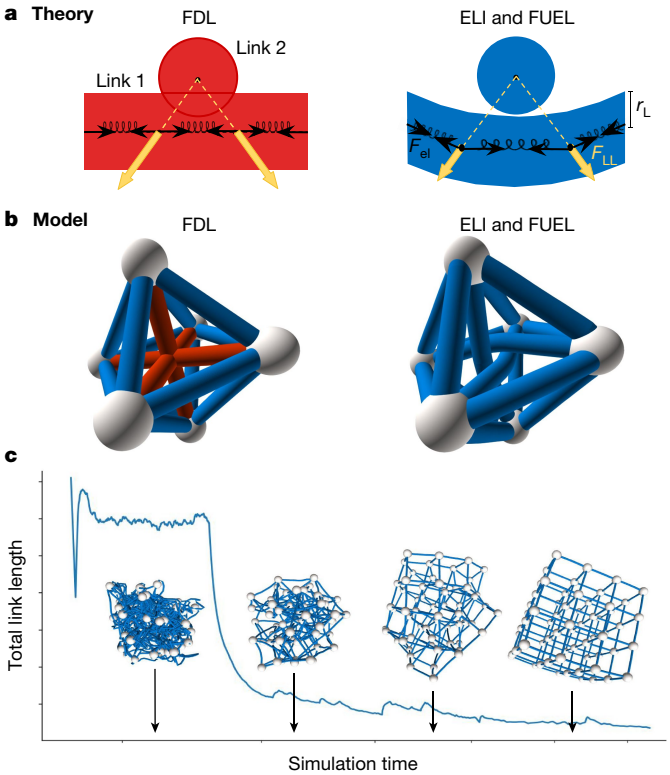

Fig. 1 | Modelling framework to avoid link and node crossings. a, We model each link as a stretched, flexible rubber band, which is represented by many short springs connected to each other, pulled apart by elastic forces F_{el}. In ELI and FUEL, the links exert a repulsive force F_{LL} on each other that falls sharply for radii larger than r_L; for the FDL, $F_{LL}=0$ and $r_L=0$. Whereas in the FDL the links may cross each other (left), in ELI and FUEL such crossings are prohibited (right). **b**, A small network with $N=6$ nodes laid out using the FDL (left), which results in multiple link crossings (red links). Laying the network out using ELI (right) resolves these crossings. **c**, Evolution of the total link length (main plot) and layout of the lattice (insets) during simulated annealing, which determines the final layout of a lattice by minimizing the total link length, starting from a random layout with $r_L \ll r_N$. The thermal noise from the annealing helps links to pass through each other to resolve crossings.

networks), sizes and link densities. We find that the networks undergo a geometric transition as we increase the link thickness (Fig. 2e–h).

For small r_L (the weakly interacting regime), the ELI and FUEL layouts are largely indistinguishable from the initial FDL. At low r_L, the average link length $\langle l\rangle$ is independent of r_L, even as r_L increases by orders of magnitude (Fig. 2b). This is unexpected, given that there is an increase by a factor of ten in the number of potential link crossings in this regime (Fig. 2a). The unchanged $\langle l\rangle$ indicates that ELI and FUEL avoid the increasing number of crossing via only a small amount of local bending of the links. Similar behaviour is seen for the average curvature of the links $\langle C\rangle$. We find that $\langle C\rangle$ changes only modestly from its value at the smallest r_L throughout the weakly interacting regime (Fig. 2c), which indicates that despite the multiple bends in some links that are necessary to avoid crossings the links remain mostly straight. Note that the behaviour of $\langle C\rangle$ in the weakly interacting regime is model-dependent: the movement of nodes in FUEL provides a way of avoiding crossings that requires less curving of the links. Altogether, we find that in the weakly interacting regime local link rearrangements are sufficient to avoid the multiple crossings that are present in the FDL.

Once r_L exceeds a critical value r_L^c (the strongly interacting regime), we observe a marked change in the geometry of the network (Fig. 2f, h). In ELI, with fixed node positions, the links must take long, convoluted routes outside the network to reach their end nodes because they are unable to find sufficient space between the nodes. This change in the link structure is particularly visible in the skeleton of the layout (white links in Fig. 2f, h). In FUEL, with flexible node positions, the links reach their destination by pushing the nodes away from each other. These changes for ELI and FUEL alter the behaviour of $\langle l\rangle$, which in the strongly interacting regime increases linearly with r_L. The change in link structure also results in relatively large changes in $\langle C\rangle$ at r_L^c; after the transition, $\langle C\rangle$ decreases as $1/r_L$. Despite the different mechanisms that underpin the two models, the scalings of $\langle l\rangle$ and $\langle C\rangle$ in the strongly interacting regime in ELI and FUEL are independent of the network topology. The linear increase in $\langle l\rangle$ and the $1/r_L$ decrease in $\langle C\rangle$ that we observe for both layout models are consistent with isometric scaling, indicating that the layouts in the strongly interacting regime are structurally similar for different r_L to each other if we rescale them by r_L (Supplementary Information section 5.A).

We determine the origin of the transition in the geometry of the networks by estimating the transition point r_L^c. When the links are much thinner than the node repulsion range r_N, the layout is dominated by the repulsive forces between the nodes, which together occupy the volume $V_N=4\sqrt{2}\,Nr_N^3/3$ (Supplementary Information section 10). When the volume occupied by the links becomes comparable to V_N, the layout must change to accommodate the links. This change induces the transition from the weakly interacting regime to the strongly interacting regime. Taking into account the volume of all nodes and links, we calculate the transition point $\tilde{r}^c=r_L^c/r_N$ to be (Supplementary Information section 10):

$$\tilde{r}^c=\frac{6A^{1/3}}{A^{2/3}+12B} \tag{3}$$

where

$$A=-12\left(3\langle k^{3/2}\rangle+\sqrt{9\langle k^{3/2}\rangle^2-12B^3}\right)$$

$$B=\left(\frac{3}{4}\right)^{1/3}\frac{cL}{N^{2/3}}$$

$$c=\frac{\langle l\rangle}{R}$$

R is the radius of the layout, k is the degree of the nodes and the average $\langle k^{3/2}\rangle$ is taken over the degree distribution of the network. In scale-free and random networks, in the limit $N\to\infty$ we obtain $\tilde{r}^c\approx aL^{-1/2}N^{1/3}$ (Supplementary Information section 10). Given that in many real and model networks $L\approx mN$ for some constant m, we obtain $\tilde{r}^c\propto N^{-1/6}$; therefore, in the limit $N\to\infty$ we find $\tilde{r}^c\to 0$, which implies that the weakly interacting regime is absent in the thermodynamic limit. In other words, in networks with a large number of nodes, the crossings are so numerous that they cannot be ignored. Consequently, the FDL and other currently used layout tools that do not consider link crossings are expected to be inappropriate for large physical networks because the layouts of such networks are dominated by crossings.

Although networks with different N and L transition at different r_L/r_N ratios, if we scale r_L/r_N by $\tilde{r}^c$ the transition occurs near unity for all networks. Using the scaling exponent of the average link length ($\phi\langle l\rangle=\mathrm{d}[\log(\langle l\rangle)]/\mathrm{d}[\log(r_L)]$) as the order parameter, the data collapse to a single curve (Fig. 2k), confirming the validity of equation (3). The fact that the transition points of networks with different topologies (scale-free and random networks, lattices and random geometric graphs; Supplementary Information section 11) exhibit similar dependences on r_L suggests that the transition shown in Fig. 2 is independent of the topology and degree distribution of the network.

Analysis of the effects of the size of the network on the scaling of the order parameter (finite-size scaling analysis) indicates that the layout transition occurs over a small, but non-zero range of r_L/r_N, regardless of the network size (Supplementary Information section 11). This result suggests that we are observing a crossover[17,18] from mean-field behaviour ($\phi\langle l\rangle=0$) to scaling behaviour ($\phi\langle l\rangle=1$). For ELI and FUEL, the weakly interacting regime is well described by an FDL with local

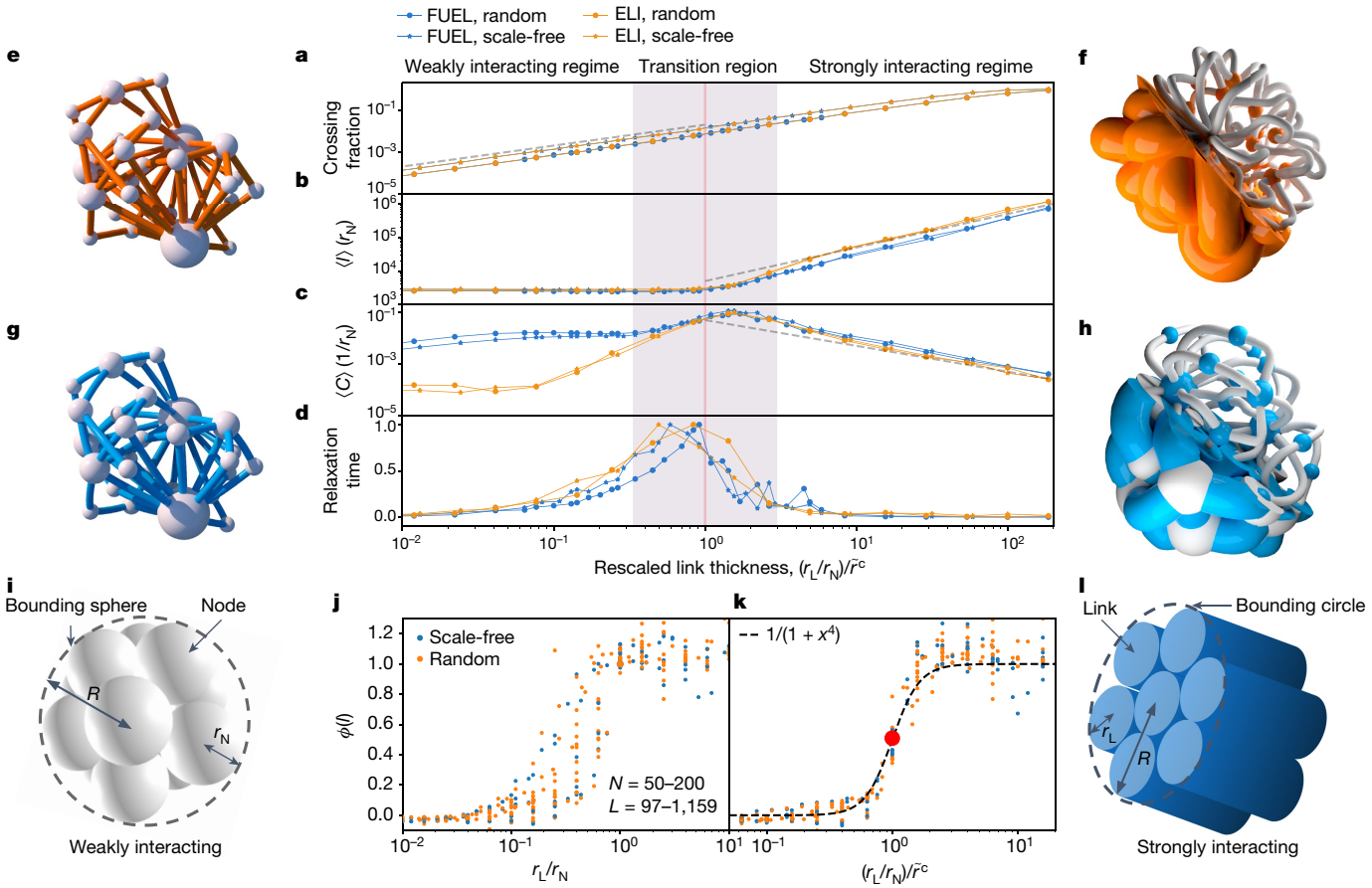

Fig. 2 | Crossover in network layouts. a, The number of link crossings in random (circles) and scale-free (stars) networks using ELI (orange) and FUEL (blue) are calculated assuming that the links are straight (that is, using the FDL), and then normalized by the total number of pairs of links to obtain the crossing fraction shown. The number of link crossings in the FDL grows linearly with r_L (grey dashed line), saturating at very high r_L. A physically realistic layout must resolve this increasing number of crossings. **b**, In all four cases, the average link length $\langle l \rangle$ remains largely constant in the weakly interacting regime, but grows linearly (dashed grey line) in the strongly interacting regime. **c**, The average link curvature $\langle C \rangle$ increases slowly in the weakly interacting regime, with FUEL exhibiting higher average curvature than ELI, then falls linearly (dashed grey line) in the strongly interacting regime. **d**, The relaxation time of the simulated annealing grows substantially near the transition point $\tilde{r}^c = r_L^c/r_N = r_L/r_N$ (vertical pink line). **e**–**h**, ELI (**e**, **f**; orange) and FUEL (**g**, **h**; blue) layouts for a Barabási–Albert network[16] with $N = 20$ nodes and minimum degree $m = 2$. When $r_L \ll r_N$, the ELI (**e**) and FUEL (**g**) layouts are similar to the FDL (not shown). For larger r_L, links bend to avoid each other: for ELI (**f**), the links do not fit inside the region containing the nodes and make outward arcs; by contrast, because nodes are free to move for FUEL (**h**), the layout behaves more gently (that is, it contains shorter links, which bend less relative to ELI). In **f** and **h**, the bottom left parts of the image show the full-scale networks and the top right parts show the node and link 'skeletons', with the colours inverted, to help to visualize the geometry. **i**, In the weakly interacting regime ($r_L \ll r_N$), the links are thin and the radius of the entire layout is approximately the radius R of the bounding sphere that surrounds the N nodes of radius r_N. **l**, At larger r_L/r_N, thick links avoid crossing each other and their volume dominates the volume of the whole layout. **j**, The order parameter $\phi(l) = \mathrm{d}[\log(\langle l \rangle)]/\mathrm{d}[\log(r_L)]$ (the scaling exponent of $\langle l \rangle \propto r_L^{\phi(l)}$) versus r_L/r_N for networks with different N (50–200) and L (97–1,159) and different geometries (orange, random; blue, scale-free). **k**, Rescaling the ratio r_L/r_N by $\tilde{r}^c$ (equation (3)) collapses the transition point, shown where $\phi(l) = 1/2$ (red circle). This transition occurs over a small range of r_L/r_N (pink shaded area in **a**–**d**) regardless of the system size, providing evidence of a crossover. The black dashed curve is a smooth fit to the order parameter.

perturbations to resolve possible link crossings. However, this regime disappears in the thermodynamic limit ($N \to \infty$). In this limit, only the strongly interacting regime is observed, which is dominated by strong link–link interactions and displays universal scaling.

The crossover that we observe also alters the physical properties of the network. For example, the response of a network to external forces is captured by the Cauchy stress tensor[19] $T_{\mu\nu} = \partial_\mu \partial_\nu V$ (Supplementary Information section 6), which depends on the physical and material properties of the nodes and links. In the weakly interacting regime the links are mostly straight; hence, the node terms V_{NN} and V_{NL} dominate the total stress. Because each node is surrounded by a varying number of other nodes, the stress does not spread uniformly in all directions but has shear (off-diagonal) components—a common feature of solids. In the strongly interacting regime, the links fill up the space; hence, the link contributions $V_{el} + V_{LL}$ dominate $T_{\mu\nu}$, resulting in a diagonal total stress tensor (Supplementary Information section 6). In other words, we predict that networks in the strongly interacting regime will display a fluid or gel-like response to external stress. To test the validity of the solid–gel transition, we compress the networks generated by FUEL in the y direction and measure the tensile forces $\sigma_\mu = T_{\mu\mu}$ (Fig. 3a; Supplementary Information section 6). We again observe a crossover at the value of $\tilde{r}^c$ predicted by equation (3) from a roughly constant stress in the weakly interacting regime to a monotonically increasing stress in the strongly interacting regime (Fig. 3b). Furthermore, as we rotate the network, we find that the stress ratio $\sigma_\parallel/\sigma_\perp$ displays large fluctuations in the weakly interacting regime—behaviour that is often observed in anisotropic solids. The fluctuations vanish at the transition point $\tilde{r}^c$ and the stress ratio settles to the hydrostatic ratio $\sigma_\parallel / \sigma_\perp = 1 / \sqrt{2}$ (Fig. 3c)—as expected for gels under pressure.

In summary, the geometry of physical networks is characterized by two distinct regimes: a weakly interacting regime, in which the overlap between the nodes and links is avoided via local link rearrangements, and a strongly interacting regime, the layout of which is shaped by the link–link expulsion. Networks in the weakly interacting regime are

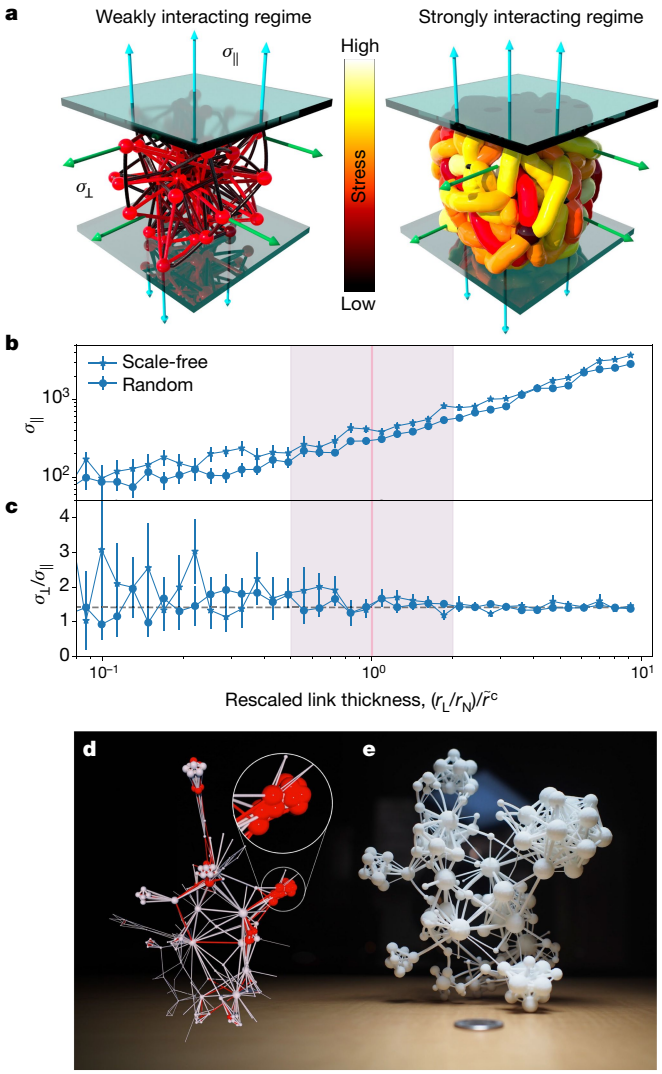

Fig. 3 | Stressed networks and 3D printing. a, The build-up of tensile stress in the nodes and links as a result of compressing the network between two walls. Arrows indicate tensile stress components: cyan, parallel to the direction of compression, $\sigma_\parallel(x)$; green, perpendicular to the direction of compression, $\sigma_\perp(x)$. The networks are coloured on the basis of the total amount of stress. In the weakly interacting regime (left), the stress is concentrated in the nodes; in the strongly interacting regime (right), almost all of the stress is in the links. **b**, The parallel stress component $\sigma_\parallel$ of scale-free (squares) and random (circles) networks as a function of scaled link thickness $(r_L/r_N)/\tilde{r}^c$. Because the definition of x, y and z is frame-dependent, we average the forces over 50 random network orientations. **c**, The ratio of parallel and transverse tensile stress components $\sigma_\perp/\sigma_\parallel$. Error bars in **b** and **c** correspond to one standard deviation around the mean, calculated over the 50 random orientations. In the weakly interacting regime, the ratio depends on the orientation of the layout (as can be seen from the large error bars from averaging over the orientations), which indicates solid-like behaviour. In the strongly interacting regime, the fluctuations in $\sigma_\perp/\sigma_\parallel$ decay, yielding a constant ratio. **d**, **e**, Visualization of networks. As an example, we consider a network with $N = 184$ and $L = 716$ that represents ingredients that share flavour compounds[21]. A three-dimensional rendering of the FDL (**d**) results in multiple crossing (red). The inset in **d** highlights a densely connected region (corresponding to dairy products) with a lot of overlap; consequently, it is difficult to discern the underlying network. By contrast, when laying out the flavour network using FUEL (**e**; printed using a commercial 3D printer), the crossings disappear, unveiling the inner structure of the network.

solid-like, whereas those in the strongly interacting regime behave like gels. The transition that we observe between the two regimes is unique to three dimensions: because links are effectively one-dimensional objects, the non-crossing condition results in knot-like constraints in three dimensions, which prevent the links from passing through each other. In four dimensions or more, knots of one-dimensional objects can be untied[20], so the non-crossing conditions will not constrain the geometry. Therefore, three is the lowest number of dimensions in which links can avoid each other by bending and the highest in which they cannot pass by each other without breaking or tunnelling.

Both regimes have applications. In contrast to the physical networks considered thus far in which the nodes and links have physical sizes, many networks, such as disease–gene interactions, are more abstract, with no real three-dimensional manifestation. In such cases, the layout of the network is not limited by the physical constraints of the system, but can be chosen in such a way to best visualize the underlying network structure. Thus, the weakly interacting regime is appropriate for network visualizations because it clearly separates nodes and links and is amenable to 3D printing, which provides a way of interacting with the network and exploring its inner structure directly. As an example, we consider a network with 184 nodes and 716 links that represents ingredients that share flavour compounds[21]. For networks such as this with high link densities, two-dimensional visualizations suffer from visual cluttering, making only a fraction of the links visible[21]. A three-dimensional layout may provide more clarity, but the FDL still exhibits node and link overlap (Fig. 3d), obstructing the details of the geometry of the network. By contrast, when applying FUEL and choosing r_L to be sufficiently small that the layout is in the weakly interacting regime, we obtain a geometry that reveals the underlying structure of the network and is amenable to 3D printing (Fig. 3e). Given that for large N link crossings in the FDL are inevitable, the method introduced here to resolve crossings will be essential as we aim to visualize large networks. Although the weakly interacting regime vanishes in the thermodynamic limit ($N \to \infty$), for a large but finite network with a fixed number of nodes we will always be able to choose r_L and r_N so that we stay in the weakly interacting regime.

The strongly interacting regime is directly relevant to the brain—a three-dimensional physical network in which the close-packing of the axons is critical to their ability to form synapses[22,23]. A scaling law of $V_w \propto A_w^{1.5}$ between the volume V_w and surface area A_w of the white matter in rodent brains has been observed previously[24]. This law implies that in these networks the average neuron length scales with the axon thickness as $\langle l \rangle = V_w / A_w \propto r_L$, as predicted for the strongly interacting regime (Fig. 2b). If we describe anatomical regions as nodes and axon bundles connecting the anatomical regions as links, then the thickness of the axon bundles r_L is comparable to the size of the anatomical regions. This result supports the prediction of the empirical scaling that these brain networks are in the strongly interacting regime. Thus, equations (1) and (2) provide an appropriate modelling framework to capture the geometry of dense neuronal networks, generating a layout that minimizes the total link length[25,26] while respecting the non-crossing conditions that axons must obey[1].

Data availability

All data used in the figures were generated using the simulation code available at https://github.com/nimadehmamy/3D-ELI-FUEL. The data that support the findings of this study are available from the corresponding author on reasonable request.

Online content

Any Methods, including any statements of data availability and Nature Research reporting summaries, along with any additional references and Source Data files, are available in the online version of the paper at https://doi.org/10.1038/s41586-018-0726-6.

Received: 28 November 2017; Accepted: 21 August 2018;
Published online 28 November 2018.

1. Kasthuri, N. et al. Saturated reconstruction of a volume of neocortex. *Cell* **162**, 648–661 (2015).
2. Oh, S. W. et al. A mesoscale connectome of the mouse brain. *Nature* **508**, 207–214 (2014).

3. Wong, S. et al. Monolithic 3D integrated circuits. In *2007 International Symposium onVLSI Technology, Systems and Applications* 1–4 (IEEE, 2007).
4. Friese, C. F. & Allen, M. F. The spread of Va mycorrhizal fungal hyphae in the soil: inoculum types and external hyphal architecture. *Mycologia* **83**, 409–418 (1991).
5. Barrat, A., Barthelemy, M. & Vespignani, A. *Dynamical Processes on Complex Networks* (Cambridge Univ. Press, Cambridge, 2008).
6. Barabási, A.-L. *Network Science* (Cambridge Univ. Press, Cambridge, 2016).
7. Albert, R. & Barabási, A.-L. Statistical mechanics of complex networks. *Rev. Mod. Phys*. **74**, 47–97 (2002).
8. Kamada, T. & Kawai, S. An algorithm for drawing general undirected graphs. *Inf. Process. Lett*. **31**, 7–15 (1989).
9. Fruchterman, T. M. & Reingold, E. M. Graph drawing by force-directed placement. *Softw. Pract. Exper*. **21**, 1129–1164 (1991).
10. Dubrovin, B., Fomenko, A. & Novikov, S. *Modern Geometry—Methods and Applications. Part II: The Geometry and Topology of Manifolds [transl. by R. G. Burns]* 371–379 (Springer, New York, 1984).
11. des Cloizeaux, J. Lagrangian theory for a self-avoiding random chain. *Phys. Rev. A* **10**, 1665–1669 (1974).
12. Mézard, M. & Parisi, G. Replica field theory for random manifolds. *J. Phys. I* **1**, 809–836 (1991).
13. Gay, J. & Berne, B. Modification of the overlap potential to mimic a linear site–site potential. *J. Chem. Phys*. **74**, 3316–3319 (1981).
14. Bouchaud, J.-P., Cugliandolo, L. F., Kurchan, J. & Mezard, M. in *Spin Glasses and Random Fields* (ed. Young, A. P.) 161–223 (World Scientific, Singapore, 1998).
15. Kirkpatrick, S., Gelatt, C. D., Jr & Vecchi, M. P. in *Spin Glass Theory and Beyond* (eds Mézard, M., Parisi, G. & Virasoro, M. A.) 339–348 (World Scientific, Singapore, 1987).
16. Barabási, A.-L. & Albert, R. Emergence of scaling in random networks. *Science* **286**, 509–512 (1999).
17. Chaikin, P. M. & Lubensky, T. C. *Principles of Condensed Matter Physics* Ch. 5.8 (Cambridge Univ. Press, Cambridge, 2000).
18. Cardy, J. *Scaling and Renormalization in Statistical Physics* Vol. 5, 67–71 (Cambridge Univ. Press, Cambridge, 1996).
19. Irgens, F. *Continuum Mechanics* 60–73 (Springer, Berlin, 2008).
20. Zeeman, E. C. Unknotting combinatorial balls. *Ann. Math*. **78**, 501–526 (1963).
21. Ahn, Y.-Y., Ahnert, S. E., Bagrow, J. P. & Barabási, A.-L. Flavor network and the principles of food pairing. *Sci. Rep*. **1**, 196 (2011).
22. Stepanyants, A., Hof, P. R. & Chklovskii, D. B. Geometry and structural plasticity of synaptic connectivity. *Neuron* **34**, 275–288 (2002).
23. Rivera-Alba, M. et al. Wiring economy and volume exclusion determine neuronal placement in the *Drosophila* brain. *Curr. Biol*. **21**, 2000–2005 (2011).
24. Ventura-Antunes, L., Mota, B. & Herculano-Houzel, S. Different scaling of white matter volume, cortical connectivity, and gyrification across rodent and primate brains. *Front. Neuroanat*. **7**, 3 (2013).
25. Bullmore, E. & Sporns, O. The economy of brain network organization. *Nat. Rev. Neurosci*. **13**, 336–349 (2012).
26. Sporns, O., Chialvo, D. R., Kaiser, M. & Hilgetag, C. C. Organization, development and function of complex brain networks. *Trends Cogn. Sci*. **8**, 418–425 (2004).

Acknowledgements We thank A. Grishchenko for 3D visualizations and photography, K. Albrecht, M. Martino and H. Sayama for discussions, and Formlabs and Shapeways for 3D printing. We were supported by grants from Templeton (award number 61066), NSF (award number 1735505), NIH (award number P01HL132825) and AHA (award number 151708).

Reviewer information *Nature* thanks G. Bianconi and the other anonymous reviewer(s) for their contribution to the peer review of this work.

Author contributions N.D. developed, ran and analysed the simulations, performed the mathematical modelling and derivations, and contributed to writing the manuscript. S.M. contributed to programming and running the simulations, generating figures, editing and 3D printing. A.-L.B. contributed to the conceptual design of the study and was the lead writer of the manuscript.

Competing interests The authors declare no competing interests.

Additional information
Supplementary information is available for this paper at https://doi.org/10.1038/s41586-018-0726-6.
Reprints and permissions information is available at http://www.nature.com/reprints.
Correspondence and requests for materials should be addressed to A.-L.B.
Publisher's note: Springer Nature remains neutral with regard to jurisdictional claims in published maps and institutional affiliations.